Ab Initio Thermodynamic Results for the Degenerate Electron Gas at Finite Temperature

T. Schoof, S. Groth, J. Vorberger, and M. Bonitz
Institut für Theoretische Physik und Astrophysik, Christian-Albrechts-Universität zu Kiel, D-24098 Kiel, Germany
(Received 17 February 2015; revised manuscript received 22 June 2015; published 22 September 2015)

The uniform electron gas at finite temperature is of key relevance for many applications in dense plasmas, warm dense matter, laser excited solids, and much more. Accurate thermodynamic data for the uniform electron gas are an essential ingredient for many-body theories, in particular, density-functional theory. Recently, first-principles restricted path integral Monte Carlo results became available, which, however, had to be restricted to moderate degeneracy, i.e., low to moderate densities with $r_s = \bar{r}/a_B \gtrsim 1$. Here we present novel first-principles configuration path integral Monte Carlo results for electrons for $r_s \leq 4$. We also present quantum statistical data within the e^4 approximation that are in good agreement with the simulations at small to moderate r_s.

DOI: 10.1103/PhysRevLett.115.130402 PACS numbers: 05.30.Fk, 71.10.Ca

Thermodynamic properties of quantum degenerate electrons are vital for the description of matter at high densities [1–3], such as dense plasmas in compact stars or planet cores [4–6], as well as in laser fusion experiments at NIF [7–9], Rochester [10], or Sandia [11,12]. Additionally, the electron component is of crucial importance for understanding the properties of atoms, molecules, and existing and novel materials. The most successful approach has been density-functional theory (DFT) combined with an approximation for the exchange-correlation potential. Its success is based on the availability of accurate zero temperature data for the uniform eledtron gas (UEG), which is obtained from analytically known limiting cases combined with first-principles quantum Monte Carlo (QMC) data [13].

In recent years more and more applications have emerged where the electrons are highly excited, e.g., by compression of the material or by electromagnetic radiation. This has led to an urgent need for accurate thermodynamic data of the UEG at finite temperature. One known limiting case is the highly degenerate ideal Fermi gas (IFG), and perturbation theory results around the IFG, starting with the Hartree-Fock and the first two correlation corrections (Montroll-Ward and e^4 approximation) [14–19], have long been known. They break down when the Coulomb interaction energy among the electrons becomes comparable to their kinetic energy, requiring computer simulations such as path integral Monte Carlo (PIMC) simulations [20]. While restricted PIMC (RPIMC) results for dense multicomponent quantum plasmas [21,22], as well as direct fermionic PIMC (DPIMC) results [23–26], have been available for 15 years, only recently finite-temperature RPIMC results for the UEG have been obtained [27]. It is well known that fermionic PIMC simulations in continuous space are hampered by the fermion sign problem (FSP), which is known to be NP hard [28]. This means, with increasing quantum degeneracy, i.e., increasing parameter $\chi = n\lambda_{DB}^3$, which is the product of density and thermal de Broglie wavelength cubed ($\lambda_{DB}^2 = h^2[2\pi m k_B T]^{-1}$), the simulations suffer an exponential loss of accuracy. The RPIMC method formally avoids the FSP by an additional assumption on the nodes of the density matrix; however, it also cannot access high densities [29], $r_s < 1$ ($r_s = \bar{r}/a_B$, where $\bar{r}$ is the mean interparticle distance, $n^{-1} = 4\pi\bar{r}^3/3$, and a_B is the Bohr radius). Also, the quality of the simulations around $r_s = 1$, at low temperatures $\Theta = k_B T/E_F \leq 1$ (E_F is the Fermi energy) is unknown. However, this leaves out the high-density range that is of high importance, e.g., for deuterium-tritium implosions at NIF where mass densities of 400 g cm^{-3} were reported [9], corresponding to $r_s \approx 0.24$; see Fig. 1.

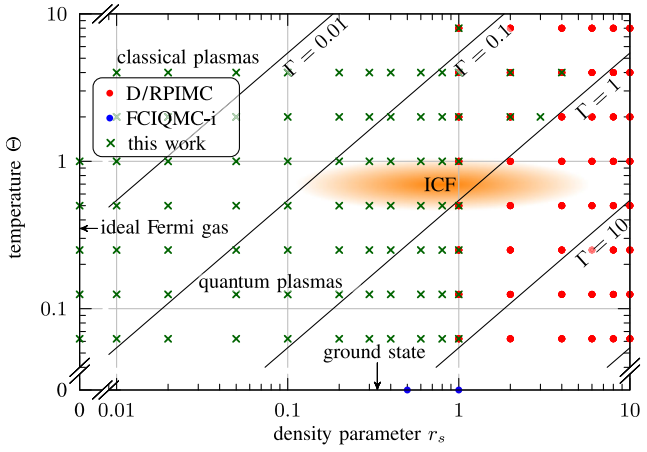

FIG. 1 (color online). Density-temperature plain in the warm dense matter range. Typical inertial confinement fusion (ICF) parameters [8]. Quantum (classical) behavior dominates below (above) the line $\Theta = 1$. $\Gamma = e^2/\bar{r}k_B T$ is the classical coupling parameter. Red dots, available finite-temperature RPIMC [27] and DPIMC [30] data for the UEG; blue dots, ground state data of Ref. [31]; green crosses, CPIMC and analytical results of this work.

The authors of Ref. [27] also performed DPIMC simulations that confirmed that, for $\Theta < 0.5$ and $r_s \lesssim 4$, these simulations are practically not possible. We also mention independent recent DPIMC simulations [30] that are overall in good agreement with the data of Ref. [27] but indicate large deviations for the lowest temperatures and $r_s \lesssim 2$. To bridge the gap between the known analytical result for the IFG ($r_s = 0$) and previous simulations ($r_s \gtrsim 1$) and to provide comprehensive input data for finite-temperature DFT, several fits have been proposed [32,33]. However, they crucially depend on the quality of the underlying simulation data.

In this Letter we present the first *ab initio* simulation results that avoid a simplified treatment of fermionic exchange for $r_s \lesssim 1$ and finite temperatures $\Theta \lesssim 1.0$. We apply the recently developed fermionic configuration path integral Monte Carlo (CPIMC) approach to the UEG and demonstrate its capabilities for 33 spin-polarized electrons in a cubic box of side length L (as was studied in Refs. [27,34]). Our simulations have no sign problem for $0 \le r_s \le 0.4$ and are accurate up to $r_s = 1, \ldots, 4$, depending on temperature.

CPIMC approach for the UEG.—The Hamiltonian in second quantization with respect to plane waves $\langle \vec{r}|\vec{k}\rangle = (1/L^{3/2})e^{i\vec{k}\cdot\vec{r}}$, with $\vec{k} = (2\pi/L)\vec{m}$, $\vec{m} \in \mathbb{Z}^3$, is (Rydberg units)

$$\hat{H} = \sum_i \vec{k}_i^2 \hat{a}_i^\dagger \hat{a}_i + 2\sum_{\substack{i<j,k<l \\ i\neq k, j\neq l}} w^-_{ijkl} \hat{a}_i^\dagger \hat{a}_j^\dagger \hat{a}_l \hat{a}_k + E_M, \quad (1)$$

with $w^-_{ijkl} = w_{ijkl} - w_{ijlk}$, $w_{ijkl} = (4\pi e^2/L^3 \vec{k}_{ik}^2)\delta_{\vec{k}_i+\vec{k}_j,\vec{k}_k+\vec{k}_l}$, where the first (second) term describes the kinetic (interaction) energy and $\vec{k}_{ik} = \vec{k}_i - \vec{k}_k$. The Madelung energy E_M accounts for the self-interaction of the Ewald summation in periodic boundary conditions [35] for which we found $E_M \approx -2.837297(3/4\pi)^{1/3} N^{2/3} r_s^{-1}$. The operator $\hat{a}_i^\dagger$ ($\hat{a}_i$) creates (annihilates) a particle in the orbital $|\vec{k}_i\rangle$. In the interaction term, the $\vec{k}_i = \vec{k}_k$ and $\vec{k}_j = \vec{k}_l$ components cancel with the interactions with the positive background. While the complete (infinite) set of plane waves $\langle \vec{r}|\vec{k}_i\rangle$ forms a basis in the single-particle Hilbert space, for simulations it has to be truncated at a number N_B of orbitals.

In conventional RPIMC and DPIMC simulations, the system (1) is treated in the coordinate representation allowing for a numerically exact description in the classical strongly coupled limit and for weak degeneracy. The CPIMC method [36], in contrast, is constructed in a way that it allows for exact simulations in the opposite limit of the ideal Fermi gas, $r_s = 0$ [37], and at weak to moderate coupling and strong to moderate degeneracy. This is achieved by representing the N-electron state in second quantization [38] as a superposition of Slater determinants, $|\{n\}\rangle = |n_1, n_2, \ldots\rangle$, with the fermionic occupation numbers, $n_i = 0, 1$, of the orbitals $|\vec{k}_i\rangle$. In this way, fermionic antisymmetry is "built in" exactly. The partition function Z and quantum-statistical expectation values, such as the internal energy U, are straightforwardly computed in Fock space as

$$Z(\Theta, r_s; N) = \mathrm{Tr}_{|\{n\}\rangle} e^{-\beta\hat{H}}, \quad (2)$$

$$U(\Theta, r_s; N) = \langle \hat{H} \rangle = Z^{-1} \mathrm{Tr}_{|\{n\}\rangle} \hat{H} e^{-\beta\hat{H}}. \quad (3)$$

The trace is evaluated using the concept of the continuous time PIMC method, which has been successfully applied to bosonic lattice models [40–43]. We have generalized this concept to continuous fermionic systems with long-range interactions [36,44]. The main idea is to split the Hamiltonian into a diagonal $\hat{D}$ and an off-diagonal part $\hat{Y}$ and to sum up the entire perturbation series of the density operator $e^{-\beta\hat{H}}$ in terms of $\hat{Y}$. The final result, for the case of the UEG, is [45]

$$Z = \sum_{\substack{K=0, \\ K\neq 1}}^{\infty} \sum_{\{n\}} \sum_{s_1 \ldots s_{K-1}} \int_0^\beta d\tau_1 \int_{\tau_1}^\beta d\tau_2 \ldots \int_{\tau_{K-1}}^\beta d\tau_K \times (-1)^K e^{-\sum_{i=0}^K D_{\{n^{(i)}\}}(\tau_{i+1}-\tau_i)} \prod_{i=1}^K (-1)^{\alpha_{s_i}} w^-_{s_i}, \quad (4)$$

$$D_{\{n^{(i)}\}} = \sum_l \vec{k}_l^2 n_l^{(i)} + \sum_{l<k} w^-_{lklk} n_l^{(i)} n_k^{(i)},$$

$$\alpha_{s_i} = \alpha^{(i)}_{pqrs} = \sum_{l=p}^{q-1} n_l^{(i-1)} + \sum_{l=r}^{s-1} n_l^{(i)}, \quad (5)$$

where $s_i = (p, q, r, s)$ and $p < q, r < s$ denotes a quadruple of pairwise different orbital indices.

Thus, the partition function is represented as a sum over β-periodic "paths" in Fock space, in imaginary time, which we illustrate in Fig. 2: For an ideal Fermi system a path is characterized by a single N-particle Slater determinant $|\{n\}\rangle$. For a correlated Fermi system the original

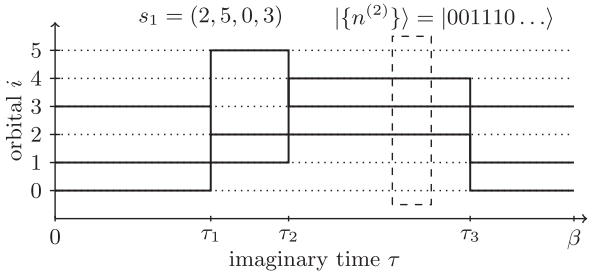

FIG. 2. Typical closed path in Slater determinant (Fock) space. The state with three occupied orbitals $|\vec{k}_0\rangle, |\vec{k}_1\rangle, |\vec{k}_3\rangle$ undergoes a two-particle excitation (s_1, τ_1) that replaces the occupied orbitals $|\vec{k}_0\rangle, |\vec{k}_3\rangle$ by $|\vec{k}_2\rangle, |\vec{k}_5\rangle$. Two further excitations occur at τ_2 and τ_3. The states at the "imaginary times" $\tau = 0$ and $\tau = \beta$ coincide. All possible paths contribute to the partition function Z, Eq. (4).

determinant $|\{n\}\rangle = |\{n^{(0)}\}\rangle$ (straight horizontal lines in Fig. 2) is interrupted by excitations of the type (s,τ): at time τ, a pair of occupied orbitals $|\vec{k}_r\rangle, |\vec{k}_s\rangle$ is replaced by the previously empty pair $|\vec{k}_p\rangle, |\vec{k}_q\rangle$. Paths differ by the number K of excitations ("kinks"), their times $\tau_1, \ldots, \tau_k$ on the τ interval $[0,\beta]$, and the involved quadruples of orbitals $s_1, \ldots, s_K$. The partition function clearly reflects this summation over the different types of kinks, integration over the kink times, and summation over K [cf. first line of Eq. (4)]. The weight of each path [terms in the second line of Eq. (4)] is determined by the Fock state matrix elements of the Hamiltonian, where diagonal elements $D_{\{n^{(i)}\}}$, Eq. (5), arise from the kinetic energy and the mean-field part of the Coulomb interaction, whereas off-diagonal elements, $(-1)^{\alpha_{s_i}} w_{s_i}^{-}$, are due to the remaining Coulomb interaction (correlation part) [46]. Expression (4) is exact for $N_B \to \infty$, allowing for *ab initio* thermodynamic simulations of the UEG.

Thermodynamic observables, such as the internal energy (3) can be cast in a form similar to Eq. (4) [45] that can be efficiently evaluated using the Metropolis Monte Carlo algorithm. To this end, we developed an ergodic algorithm that generates all possible paths in Slater determinant space. For the UEG, a total of 6 different steps are required, including addition and removal of a single kink and pairs of kinks, modification of an existing kink, and excitation of single orbitals; for details, see Ref. [45].

Numerical results.—Our CPIMC algorithm was extensively tested for Coulomb interacting fermions in a 1D harmonic trap [36]. A first test of the present algorithm for the UEG for $N = 4$ particles showed excellent agreement with exact diagonalization data [45] and was exactly reproduced by independent density matrix QMC calculations [47]. Here, we extend these simulations to $N = 33$ particles. First, we check the convergence with respect to the basis size N_B and show a typical case in Fig. 3(a) for $r_s = 0.4$. The scaling with respect to $x = 1/N_B^{-5/3}$ [48] allows for a reliable extrapolation to $x \to 0$ and to set N_B to 2109 for all simulations, giving a relative basis incompleteness error not exceeding the statistical error (1σ standard deviation).

With these parameters, we have performed extensive *ab initio* CPIMC simulations (the only approximation being the choice of N_B) for the ideal and weakly coupled UEG, up to $r_s \sim 0.4$. For larger r_s, we observe a rapid decrease of the average sign, in analogy to the harmonic oscillator case [36]. This gives rise to convergence problems of the MC algorithm in case a path with many kinks is attempted. We, therefore, introduce an artificial kink potential in Eq. (4), $V_\kappa(K) = [e^{-(\kappa+0.5-K)}+1]^{-1}$, for calculations with $r_s > 0.4$, yielding the correct partition function in the limit $\kappa \to \infty$. Performing simulations for different κ, we generally observe a rapid convergence of the total energy allowing for an extrapolation to $1/\kappa \to 0$. This is demonstrated for a particularly difficult case in Fig. 3(b). The asymptotic value and the error estimate are computed from the two extreme cases of a horizontal and linear extrapolation. With this procedure the simulations could be extended to $r_s = 1$, with the total error not exceeding 0.15%.

Our results for the exchange-correlation energy per electron E_{xc} are summarized in Fig. 4. The data cover the whole range $0 \le r_s \le 1$ and include the ideal Fermi gas where $E_{\mathrm{xc}} r_s \to$ const (Hartree-Fock limit). A detailed table

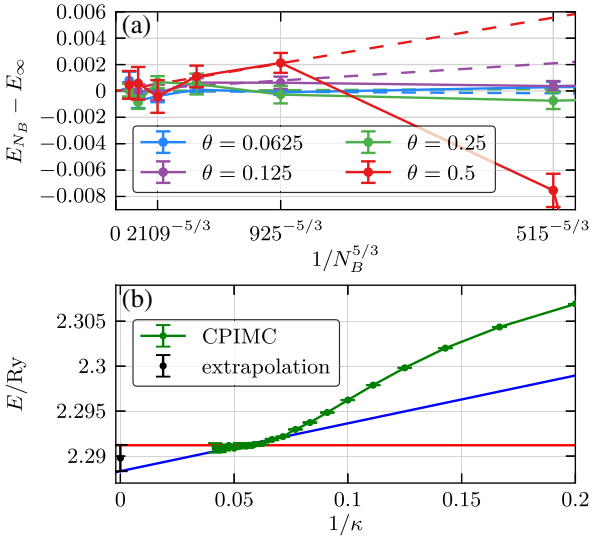

FIG. 3 (color online). Convergence of the CPIMC simulations. (a) Convergence with the single-particle basis size N_B for $r_s = 0.4$. The expected scaling with $N_B^{5/3}$ [48] is well reproduced. (b) Convergence with respect to the kink potential parameter κ (see text) and extrapolation to $1/\kappa \to 0$, corresponding to $K \to \infty$, for $r_s = 1.0$ and $\theta = 0.0625$. The asymptotic value is enclosed between the red line and the blue line.

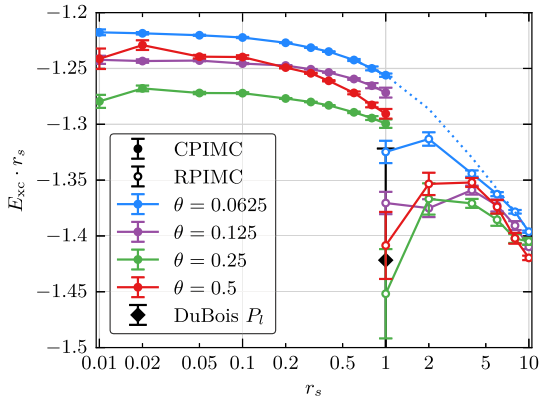

FIG. 4 (color online). Exchange-correlation energy (times r_s) for 33 spin-polarized electrons and four temperatures. Comparison of our CPIMC results (full symbols with error bars [53]) and RPIMC results of Ref. [27] (open symbols). The dotted line is an interpolation between the CPIMC and RPIMC data for $\Theta = 0.0625$. Also shown is the data point of DuBois *et al.* [34] for $\Theta = 0.125$.

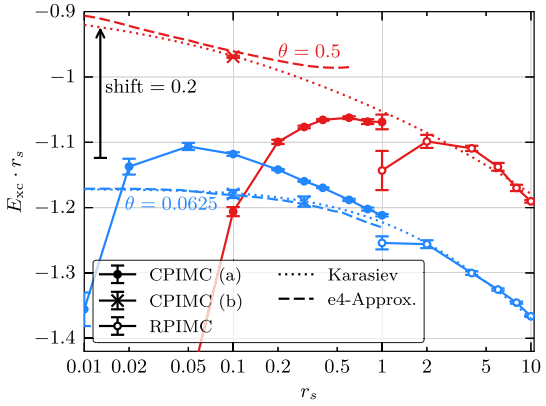

FIG. 5 (color online). Exchange correlation energy of the macroscopic polarized UEG at $\Theta = 0.0625$ (blue) and $\Theta = 0.5$ (red). Open symbols, RPIMC results [27]. CPIMC (a), our results with FSC from Ref. [54]. CPIMC (b), our data (3 points) with numerical extrapolation $N \to \infty$ [57]. Dashes, analytical e^4 approximation [49]; dots, fit of Ref. [32]. For better visibility, the curves for $\Theta = 0.5$ are up-shifted by 0.2.

of the various energy contributions as well as additional data for larger values of Θ and r_s are presented in the Supplemental Material [49]. A nontrivial observation is the nonmonotonic temperature dependence (cf. crossing of the red and pink curves) that is in agreement with RPIMC calculations and the macroscopic fit of Ref. [32]. Interestingly, all curves seem to cross over smoothly into the RPIMC data [27,50], for $r_s \gtrsim 4$, as indicated by the dotted line. There is an obvious mismatch in the range $r_s \sim 1$–4. Since our curves are accurate within the given error, this discrepancy is expected to be due to the (unknown) systematic error involved in the RPIMC method [51]. Also, the energy obtained by DuBois *et al.* [34], for $r_s = 1$ and $\Theta = 0.125$, is found to be too low.

Macroscopic results.—Predictions for a macroscopic system, based on data for just 33 particles, will inevitably lead to a loss of accuracy. Brown *et al.* published finite size corrections (FSC) in the Supplemental Material of Ref. [27], whereas a ground state formula [FSC(a)] has been presented in Ref. [54]. We tested both FSCs, after incorporating a twist-averaging procedure in our simulations [55]. For the lowest temperature, $\Theta = 0.0625$ and $r_s = 1$, FSC(a) leads to reasonable agreement with analytical approximations (see below), and smoothly connects to the RPIMC data, for $r_s \gtrsim 5$, cf. Fig. 5. For smaller r_s and higher Θ, the formula is not applicable. On the other hand, the FSC of Brown produces energies that are systematically too high [56]. Because of the lack of applicable high-density FSC, we performed additional CPIMC simulations for particle numbers up to $N_{\max} = 800$, allowing for an extrapolation to the macroscopic limit, for $r_s = 0.1$ and $\Theta = 0.0625; \Theta = 0.5$ [49]. For $\Theta = 0.0625$, an additional point at $r_s = 0.3$ could be obtained [57], cf. the crosses in Fig. 5. These accurate data will be a suitable starting point for the construction of FSC formulas that are applicable at high densities.

To obtain independent analytical results for the macroscopic UEG, we now compute $E_{\rm xc}$ including, in addition to Hartree-Fock [15], the two second order diagrams (Montroll Ward and e^4) [49]. The two results (cf. Fig. 5) converge for low r_s, eventually reaching the Hartree-Fock asymptote (horizontal line), whereas for $r_s \gtrsim 0.1$ they start to deviate from one another, and we expect the exact result to be enclosed between the two [49]. Reliable predictions are possible up to $r_s \sim 0.8$, for $\Theta = 0.0625$, and $r_s \sim 0.55$, for $\Theta = 0.5$ [49]. In Fig. 5 we also include the fit of Ref. [32] that shows, overall, a very good behavior, but is too low at $r_s \to 0$, with the deviations growing with Θ [49].

To summarize, we have presented first-principles configuration PIMC results for the UEG at finite temperature that have no sign problem at high to moderate degeneracy, $r_s \lesssim 0.4$, and allow for reliable predictions up to $r_s = 4$. This makes CPIMC simulations a perfect complementary approach to direct fermionic PIMC and to RPIMC simulations that cannot access high densities, and our results indicate that the previous RPIMC data are not reliable for $r_s \lesssim 4$. The present results will be important for dense quantum plasmas at finite temperatures that are relevant for warm dense matter, in general, and for inertial confinement fusion (ICF), in particular. Since here the electrons are typically unpolarized, we tested our CPIMC approach for this case. Although the sign problem is more severe than for the polarized situation, the CPIMC approach is well capable of producing very accurate *ab initio* finite-temperature results that smoothly connect to available $T = 0$ data [49].

Finally, the obtained accurate exchange-correlation energies provide benchmarks for finite temperature DFT, RPIMC [27], novel independent QMC simulations [34,48,52] and analytical fits [32]. Even though the fermion sign problem is not removed, the proposed combination of the CPIMC approach with the DPIMC approach (or the RPIMC approach) provides, for the UEG, a practical way to avoid it.

We acknowledge stimulating discussions with T. Dornheim, J. W. Dufty, V. Filinov, V. V. Karasiev, and S. Trickey, and we acknowledge E. Brown for providing information on the FSC(a) used in Ref. [27]. This work is supported by the Deutsche Forschungsgemeinschaft via Grant No. BO1366/10 and by Grant No. SHP006 for supercomputing time at the HLRN.

[1] L. B. Fletcher *et al.*, Observations of Continuum Depression in Warm Dense Matter with X-Ray Thomson Scattering, Phys. Rev. Lett. **112**, 145004 (2014).
[2] D. Kraus *et al.*, Probing the Complex Ion Structure in Liquid Carbon at 100 GPa, Phys. Rev. Lett. **111**, 255501 (2013).
[3] S. Regan *et al.*, Inelastic X-Ray Scattering from Shocked Liquid Deuterium, Phys. Rev. Lett. **109**, 265003 (2012).

[4] M. D. Knudson, M. P. Desjarlais, R. W. Lemke, T. R. Mattsson, M. French, N. Nettelmann, and R. Redmer, Probing the Interiors of the Ice Giants: Shock Compression of Water to 700 GPa and 3.8 g/cm^3, Phys. Rev. Lett. **108**, 091102 (2012).
[5] B. Militzer, W. B. Hubbard, J. Vorberger, I. Tamblyn, and S. A. Bonev, A massive core in Jupiter predicted from first-principles simulations, Astrophys. J., **688**, L45 (2008).
[6] N. Nettelmann, A. Becker, B. Holst, and R. Redmer, Jupiter models with improved *ab initio* hydrogen equation of state (H-REOS.2), Astrophys. J. **750**, 52 (2012).
[7] J. D. Lindl, P. Amendt, R. L. Berger, S. Gail Glendinning, S. H. Glenzer, S. W. Haan, R. L. Kauffman, O. L. Landen, and L. J. Suter, The physics basis for ignition using indirect-drive targets on the National Ignition Facility, Phys. Plasmas **11**, 339 (2004).
[8] S. X. Hu, B. Militzer, V. N. Goncharov, and S. Skupsky, First-principles equation-of-state table of deuterium for inertial confinement fusion applications, Phys. Rev. B **84**, 224109 (2011).
[9] O. Hurricane *et al.*, Fuel gain exceeding unity in an inertially confined fusion implosion, Nature (London) **506**, 343 (2014).
[10] R. Nora *et al.*, Gigabar Spherical Shock Generation on the OMEGA Laser, Phys. Rev. Lett. **114**, 045001 (2015).
[11] M. R. Gomez *et al.*, Experimental Demonstration of Fusion-Relevant Conditions in Magnetized Liner Inertial Fusion, Phys. Rev. Lett. **113**, 155003 (2014).
[12] P. F. Schmidt *et al.*, Understanding Fuel Magnetization and Mix Using Secondary Nuclear Reactions in Magneto-Inertial Fusion, Phys. Rev. Lett. **113**, 155004 (2014).
[13] D. M. Ceperley and B. J. Alder, Ground State of the Electron Gas by a Stochastic Method, Phys. Rev. Lett. **45**, 566 (1980).
[14] M. Gell-Mann and K. A. Brueckner, Correlation Energy of an Electron Gas at High Density, Phys. Rev. **106**, 364 (1957).
[15] H. E. DeWitt, Thermodynamic functions of a partially degenerate fully ionized gas, J. Nucl. Energy C **2**, 27 (1961).
[16] W. D. Kraeft and W. Stolzmann, Thermodynamic functions of Coulomb systems, Physica (Amsterdam) **97A**, 306 (1979).
[17] W. D. Kraeft, D. Kremp, W. Ebeling, and G. Röpke, *Quantum Statistics of Charged Particle Systems* (Akademie-Verlag, Berlin, 1986).
[18] D. Kremp, M. Schlanges, and W. D. Kraeft, *Quantum Statistics of Nonideal Plasmas* (Springer, New York, 2005).
[19] J. Vorberger, M. Schlanges, and W.-D. Kraeft, Equation of state for weakly coupled quantum plasmas, Phys. Rev. E **69**, 046407 (2004).
[20] D. M. Ceperley, Path integrals in the theory of condensed helium, Rev. Mod. Phys. **67**, 279 (1995).
[21] B. Militzer and R. Pollock, Variational density matrix method for warm, condensed matter: Application to dense hydrogen, Phys. Rev. E **61**, 3470 (2000).
[22] B. Militzer, First Principles Calculations of Shock Compressed Fluid Helium, Phys. Rev. Lett. **97**, 175501 (2006).
[23] V. S. Filinov, M. Bonitz, and V. E. Fortov, High density phenomena in hydrogen plasma, JETP Lett. **72**, 245 (2000).
[24] V. S. Filinov, M. Bonitz, W. Ebeling, and V. E. Fortov, Thermodynamics of hot dense H-plasmas: Path integral Monte Carlo simulations and analytical approximations, Plasma Phys. Controlled Fusion **43**, 743 (2001).
[25] A. Filinov, V. Golubnychiy, M. Bonitz, W. Ebeling, and J. W. Dufty, Temperature-dependent quantum pair potentials and their application to dense partially ionized hydrogen plasmas, Phys. Rev. E **70**, 046411 (2004).
[26] M. Bonitz, V. S. Filinov, V. E. Fortov, P. R. Levashov, and H. Fehske, Crystallization in Two-Component Coulomb Systems, Phys. Rev. Lett. **95**, 235006 (2005).
[27] E. W. Brown, B. K. Clark, J. L. DuBois, and D. M. Ceperley, Path-Integral Monte Carlo Simulation of the Warm Dense Homogeneous Electron Gas, Phys. Rev. Lett. **110**, 146405 (2013).
[28] M. Troyer and U.-J. Wiese, Computational Complexity and Fundamental Limitations to Fermionic Quantum Monte Carlo Simulations, Phys. Rev. Lett. **94**, 170201 (2005).
[29] While RPIMC simulations avoid the fermion sign problem, they fail to reproduce the ideal Fermi gas limit, as was shown by V. Filinov, Cluster expansion for ideal Fermi systems in the 'fixed-node approximation', J. Phys. A **34**, 1665 (2001); Analytical contradictions of the fixed-node density matrix, High Temp. **52**, 615 (2014).
[30] V. S. Filinov, M. Bonitz, Zh. Moldabekov, and V. E. Fortov, Fermionic path integral Monte Carlo results for the uniform electron gas at finite temperature, Phys. Rev. E **91**, 033108 (2015).
[31] J. J. Shepherd, G. H. Booth, A. Grüneis, and A. Alavi, Full configuration interaction perspective on the homogeneous electron gas, Phys. Rev. B **85**, 081103(R) (2012).
[32] V. V. Karasiev, T. Sjostrom, J. Dufty, and S. B. Trickey, Accurate Homogeneous Electron Gas Exchange-Correlation Free Energy for Local Spin-Density Calculations, Phys. Rev. Lett. **112**, 076403 (2014) and Supplemental Material therein.
[33] E. W. Brown, J. L. DuBois, M. Holzmann, and D. M. Ceperley, Exchange-correlation energy for the three-dimensional homogeneous electron gas at arbitrary temperature, Phys. Rev. B **88**, 081102(R) (2013); **88**, 199901(E) (2013).
[34] J. L. DuBois, B. J. Alder, and E. W. Brown, Overcoming the fermion sign problem in homogeneous systems, arXiv:1409.3262.
[35] L. M. Fraser and W. M. C. Foulkes, Finite-size effects and Coulomb interactions in quantum Monte Carlo calculations for homogeneous systems with periodic boundary conditions, Phys. Rev. B **53**, 1814 (1996).
[36] T. Schoof, M. Bonitz, A. Filinov, D. Hochstuhl, and J. W. Dufty, Configuration path integral Monte Carlo, Contrib. Plasma Phys. **51**, 687 (2011).
[37] In this Letter we restrict ourselves to the nonrelativistic jellium model.
[38] This concept is also used in zero temperature full configuration Monte Carlo simulations [31,39].
[39] J. J. Shepherd, G. H. Booth, and A. Alavi, Investigation of the full configuration interaction quantum Monte Carlo method using homogeneous electron gas models, J. Chem. Phys. **136**, 244101 (2012).
[40] N. V. Prokofev, B. V. Svistunov, and I. S. Tupitsyn, Exact quantum Monte Carlo process for the statistics of discrete

systems, Pisma Zh. Exp. Teor. Fiz. **64**, 853 (1996) [JETP Lett. **64**, 911 (1996)].

[41] N. V. Prokofev, B. V. Svistunov, and I. S. Tupitsyn, Exact, complete and universal continuous-time worldline Monte Carlo approach to the statistics of discrete quantum systems, J. Exp. Theor. Phys. **87**, 310 (1998).

[42] K. Van Houcke, S. M. A. Rombouts, and L. Pollet, Quantum Monte Carlo simulation in the canonical ensemble at finite temperature, Phys. Rev. E **73**, 056703 (2006).

[43] S. M. A. Rombouts, K. Van Houcke, and L. Pollet, Loop Updates for Quantum Monte Carlo Simulations in the Canonical Ensemble, Phys. Rev. Lett. **96**, 180603 (2006).

[44] S. Groth, T. Schoof, and M. Bonitz, in *Complex Plasmas: Scientific Challenges and Technological Opportunities*, edited by M. Bonitz, K. Becker, J. Lopez, and H. Thomsen (Springer, New York, 2014).

[45] T. Schoof, S. Groth, and M. Bonitz, Towards *ab initio* thermodynamics of the electron gas at strong degeneracy, Contrib. Plasma Phys. **55**, 136 (2015).

[46] Because of momentum conservation, only two-particle excitations s_i are possible (for the general case, see Ref. [44]), and the restriction to closed paths requires $K \neq 1$.

[47] Reference [48] reports *exact* agreement with our data for $N = 4$.

[48] F. D. Malone, N. S. Blunt, J. J. Shepherd, D. K. K. Lee, J. S. Spencer, and W. M. C. Foulkes, Interaction picture density matrix quantum Monte Carlo, J. Chem. Phys. **143**, 044116 (2015).

[49] See Supplemental Material at http://link.aps.org/supplemental/10.1103/PhysRevLett.115.130402 for comprehensive tables of CPIMC data, details on finite-size corrections, and analytic approximations.

[50] The RPIMC data for $N = 33$ were obtained by applying, to the total energy of Ref. [27], the finite size corrections given in the Supplemental Material of Ref. [27] and subtracting the energy of the corresponding ideal system.

[51] This is confirmed by novel independent permutation blocking PIMC [52] results for the UEG of T. Dornheim, T. Schoof, S. Groth, A. Filinov, and M. Bonitz, http://arxiv.org/abs/1508.03221.

[52] T. Dornheim, S. Groth, A. Filinov, and M. Bonitz, Permutation blocking path integral Monte Carlo: A highly efficient approach to the simulation of strongly degenerate non-ideal fermions, New J. Phys. **17**, 073017 (2015).

[53] The fluctuations of E_{xc} at small r_s arise from the vanishing of E_{xc}, compared to the total energy, for $r_s \to 0$. The latter is always well converged.

[54] N. D. Drummond, R. J. Needs, A. Sorouri, and W. M. C. Foulkes, Finite-size errors in continuum quantum Monte Carlo calculations, Phys. Rev. B **78**, 125106 (2008).

[55] C. Lin, F. H. Zong, and D. M. Ceperley, Twist-averaged boundary conditions in continuum quantum Monte Carlo algorithms, Phys. Rev. E **64**, 016702 (2001).

[56] Since the FSC of Brown *et al.* was applied without twist averaging, we used our original data for $N = 33$ for comparison.

[57] For $r_s = 0.3$ the extrapolation to $N = 150$ was achieved with an additional approximation that includes only even kink numbers. It is found to be accurate for low temperatures.